ACS APPLIED POLYMER MATERIALS

pubs.acs.org/acsapm Article

Polymer Membrane Hydrolysis Diffusion-Induced Anisotropic Hydrogel Actuator with Fast Response and Programmable Actuation

Ruofei Wang, Lin Cheng,* Chengnan Qian, Huaping Wu,* and Aiping Liu*

Cite This: ACS Appl. Polym. Mater. 2024, 6, 5890−5899 Read Online

ACCESS | Metrics & More | Article Recommendations | Supporting Information

ABSTRACT: Smart hydrogel materials have demonstrated significant advantages in application fields, such as drug delivery, tissue engineering, and smart sensing. However, developing a stimuli-responsive hydrogel that is simple to prepare, programmable, and capable of rapid response remains a challenge. Herein, we employed a polyvinyl alcohol (PVA) polymer film to hydrolyze and diffuse in a hydrogel monomer precursor solution, thereby constructing a diffusion layer and preparing an anisotropic hydrogel with a multiphase gradient structure. The diffusion-generated gradient structure creates a significant structural difference between the diffused and nondiffused layers similar to that of a bilayer structure, which leads to a significant difference in internal stress between the two layers, thus providing the hydrogel with a fast response capability (bending deformation of 527.3° in 30 s) while avoiding the interfacial confinement caused by the bilayer structure. In addition, the abundant hydroxyl groups of PVA, forming hydrogen bonding interactions with the amide groups of Poly(N-isopropylacrylamide) (PNIPAM), significantly enhance the mechanical properties of the gradient hydrogel. This enhancement is evidenced by an increase in tensile stress from 32 to 176 kPa and an increase in Young's modulus from 2.23 to 44.19 kPa. It is important to emphasize that by designing the shape of the PVA film, precise multidimensional programmable deformation can be achieved. This simple yet versatile diffusion-driven strategy offers a practical approach to the design of responsive hydrogels, potentially paving the way for future advancements in intelligent actuators, artificial muscles, and intelligent human-machine technologies.

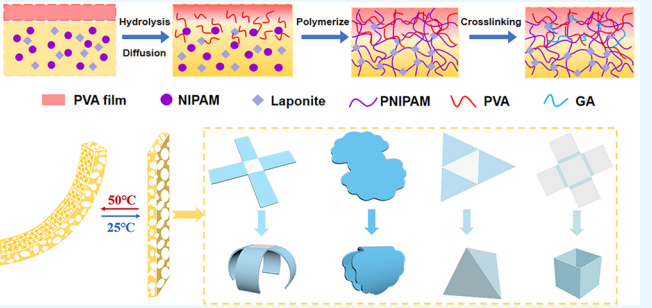

KEYWORDS: *Gradient structure, Anisotropic hydrogel, Hydrolytic diffusion, Programmable drive, Actuator*

1. INTRODUCTION

Intelligent actuators, capable of responding to specific external environmental stimuli such as temperature,[1−3] magnetic field,[4−6] electric field,[7−9] pH,[10,11] light,[12−14] ions,[15,16] etc. and converting these stimuli into mechanical energy, have garnered significant attention in various fields. In particular, among various smart materials, stimulus-responsive smart hydrogel materials hold great value in the fabrication of intelligent actuators.[17,18] Recent research has successfully demonstrated the diverse applications of these materials in soft robots,[19−21] microfluidic valves,[22,23] drug delivery systems,[24,25] multifunctional sensors,[26−30] and intelligent actuators.[31−33] However, traditional hydrogel actuators are limited as they can only produce isotropic macroscopic expansion or contraction in response to external stimuli, thereby lacking the capability for complex deformations. To address this, making hydrogels that produce characteristic deformations usually requires the rational design and fabrication of heterogeneous structures, such as building double layers.[34−37] Bilayer hydrogels typically consist of a stimulus-responsive hydrogel as a driving layer and a nonresponsive polymer as a passive layer. Yet, the mismatch in the bilayer structure affects the responsiveness of the hydrogel to some extent, and the low viscosity between the two-layer interfaces may lead to delamination along the weak interface after multiple actuations.[38]

As an alternative, constructing hydrogels with gradient structures is another effective approach.[39−41] For example, Liu et al.[42] introduced magnetic nanoparticles (MNP) within the hydrogel and designed the gradient distribution of MNP to achieve programmable responsive deformation of the hydrogel through modulation of the applied magnetic field during polymerization. However, the incompatibility of metal particles with organic materials can affect the stabilization of the

Received: February 20, 2024
Revised: May 6, 2024
Accepted: May 12, 2024
Published: May 15, 2024

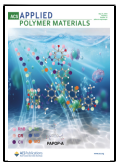

https://doi.org/10.1021/acsapm.4c00536
ACS Appl. Polym. Mater. 2024, 6, 5890−5899

hydrogel mechanical and actuation properties. In a different approach, Tan et al.[43] used Laponite nanoparticles as a cross-linking agent. Under electric field stimulation, Laponite tended to move closer to the anode, inducing a gradient structure in the hydrogel network through the gradient distribution of the cross-linking agent. This results in the hydrogel having fast stimulus responsiveness and good toughness in the high cross-linking density region, but it also leads to a limitation as the deformation is single, making it difficult to achieve complex deformations such as folding and twisting. Furthermore, Dong et al.[44] introduced an innovative approach for fabricating a heterogeneous porous hydrogel, utilizing various liquid diffusions (namely amyl alcohol, water, and ethanol) into a monomeric precursor solution designated for hydrogel synthesis. This method notably results in hydrogels characterized by significant variations in pore size along the thickness dimension, which, in turn, enhances the hydrogel's responsiveness and speed of actuation. Li et al.[45] prepared VSNPs-P(NIPAM-*co*-AA) hydrogel and VSNPs-PAA-Fe^{3+} hydrogel, respectively. The gradient hydrogel is formed by the fusion of the two layers via a self-healing action. The well-integrated gradient hydrogels obtained by this method exhibit an ultrafast thermal response and high strength, but the preparation process is overly complex. Consequently, it remains a challenge to design a simple and versatile method to obtain non-homogeneous hydrogels that exhibit fast actuation, complex deformation, and excellent mechanical properties.

Inspired by the diffusion phenomenon of molecular thermal motion, we developed a diffusion-type gradient porous anisotropic structural hydrogel actuator. This was achieved by meticulously controlling the hydrolysis and diffusion process of the polyvinyl alcohol (PVA) film in the N-isopropylacrylamide (NIPAM) hydrogel monomer precursor solution. As a result of this process, the diffusion-type hydrogel gradient structure emerges as the PVA membrane is hydrolyzed and diffuses into the hydrogel precursor solution. Consequently, the diffusion-generated gradient structure creates a significant structural difference between the diffused and nondiffused layers similar to that of a bilayer structure, which may lead to a significant difference in internal stress between the two layers, thus providing the hydrogel with a fast response capability while avoiding the interfacial confinement caused by the bilayer structure. In our experimental setup, the microstructure of the hydrogel can be further fine-tuned by adjusting the hydrolysis diffusion time of the PVA film, thereby modifying its temperature-sensitive response characteristics and driving performance. Notably, during the UV light-induced gel formation process, an abundance of hydroxyl groups in PVA forms additional intermolecular hydrogen bonds with the amide groups in PNIPAM, significantly enhancing the hydrogel's mechanical properties. Based on this, programmable motion of smart hydrogels was achieved by creating a localized porous structure in the hydrogel. This innovative approach, leveraging simple interfacial diffusion principles, realizes the three-dimensional structure and bionic motion in functional hydrogel materials, marking a frontier in the development of cutting-edge composite hydrogels.

2. MATERIALS AND METHODS

2.1. Chemicals and Supplies. Purchased from Shanghai Aladdin Chemical Co., Ltd. in China, NIPAM (purity of 99%) was utilized as the primary monomer after being refined through recrystallization. The synthetic clay, Laponite XLG ($[Mg_{5.34}Li_{0.66}Si_8O_{20}(OH)_4]Na_{0.66}$), sourced from Rockwood Chemicals Co., Ltd. in China, underwent a drying process at 125 °C for 2 h before use. Other chemicals acquired from the same supplier included 1-hydroxycyclohexyl phenyl ketone (Irg.184), polyvinyl alcohol 1788, methanol, and glutaraldehyde, all of which were used as received without further purification. Analytical grade reagents were employed in their original form. Experiments were conducted using deionized water (18.2 MΩ at 25 °C), which was obtained from a Milli-Q Plus water purification system by Millipore.

2.2. Preparation of the PVA Film. To prepare the PVA film, a solution containing 1 wt % PVA in distilled water was heated to 60 °C until the PVA was fully dissolved. The resultant solution was then poured into a polystyrene dish to form films. Upon drying, these films achieved a thickness of close to 20 μm. The drying process was carried out at 60 °C over a period of 24 h.

2.3. Preparation of the Gradient Structured Hydrogel. To create a distinctive aqueous solution with NIPAM monomers, cross-linker (Laponite XLG), and photoinitiator (Irg.184), the process began by uniformly dispersing Laponite XLG clay in water. The mixture was agitated for 2 h until it reached a clear state. Following this, NIPAM monomers were incorporated into the now clear clay mixture and the entire solution was stirred in an ice−water bath for an additional 2 h. The proportions of both clay and NIPAM monomer were meticulously maintained at 33×10^{-2} mol L^{-1} and 1.0 mol L^{-1}, respectively. Concurrently, in a separate preparation, 2.26 mg of Irg.184 was dissolved into 100 μL of methanol under cold conditions, serving as the photoinitiator, with a calculated weight percentage of 0.2% relative to the monomer. This photoinitiator mixture was then integrated into the primary solution. This blend was then carefully transferred into a specifically dimensioned mold (40 mm × 10 mm × 1 mm), constructed from glass slides and silicone. A PVA film was gently laid on top of the solution within the mold to facilitate a controlled hydrolysis process. As the hydrolysis and diffusion time increased from 10, 20, 30, 60 to 120 min, the PNIPAM hydrogel samples with different gradient structures were defined as $[PVA]_x$PNIPAM (x = 1, 2, 3, 4, 5, respectively). The solution-filled mold was exposed to UV light (365 nm) for 5 min while situated in an ice−water bath to complete the polymerization process. Subsequently, the formed hydrogel was immersed in a 1% GA solution for 10 h to chemically cross-link PVA and stabilize its structure. The fabrication of $[PVA]_x$PNIPAM hydrogels was concluded by an extensive purification process using an abundance of ethanol and water. This step ensured the removal of any residual unreacted substances from the hydrogels.

2.4. Characterization of the Composite Hydrogel. The morphological characteristics of the sample surfaces and cross-sections were meticulously examined using a field-emission scanning electron microscope (SEM, model S-4800 from Hitachi, Tokyo, Japan) operating at a low acceleration voltage of 3 kV to preserve sample integrity. Prior to these observations, the samples underwent a preparation process that included a rapid freezing phase in liquid nitrogen followed by a comprehensive freeze-drying phase extending beyond 24 h at a temperature of −80 °C, utilizing a freeze-dryer provided by Shanghai Leewen Scientific Instrument Co., Ltd. To analyze the chemical composition and bonding, Fourier transform infrared (FTIR) spectroscopy was employed using a Nicolet 6700 spectrometer. The measurements were conducted with samples prepared on potassium bromide (KBr) disks, covering a broad scanning spectrum from 450 to 4000 cm^{-1}. The thermal behavior of the hydrogel, particularly its volume phase transition temperature, was assessed using a differential scanning calimeter (DSC, model TA DSC Q200 from the USA). This analysis involved a controlled heating of the hydrogel sample from 25 to 50 °C at a uniform rate of 5 °C per minute under a nitrogen atmosphere. Mechanical properties, specifically the tensile strength of the hydrogels, were evaluated after cutting the samples into rectangular test pieces (40 mm × 10 mm). These tests were conducted by using a mechanical testing machine (model Instron 5943, USA) at a constant displacement rate of 30 mm per minute. The calculation of the Young's modulus for each sample was derived from the initial slope of the stress−strain

https://doi.org/10.1021/acsapm.4c00536
ACS Appl. Polym. Mater. 2024, 6, 5890−5899

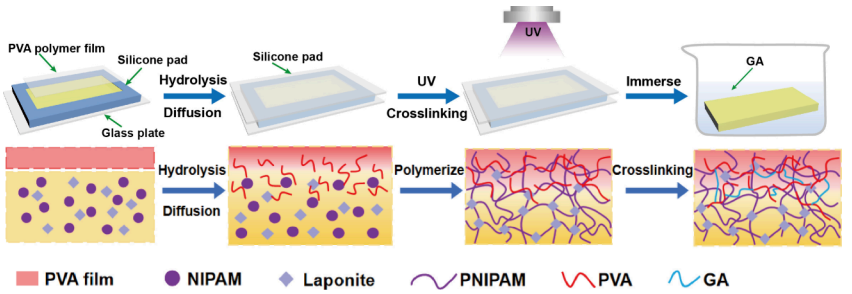

Figure 1. Schematic illustration of the synthesis of the heterogeneous [PVA]PNIPAM hydrogel induced by a polymer membrane.

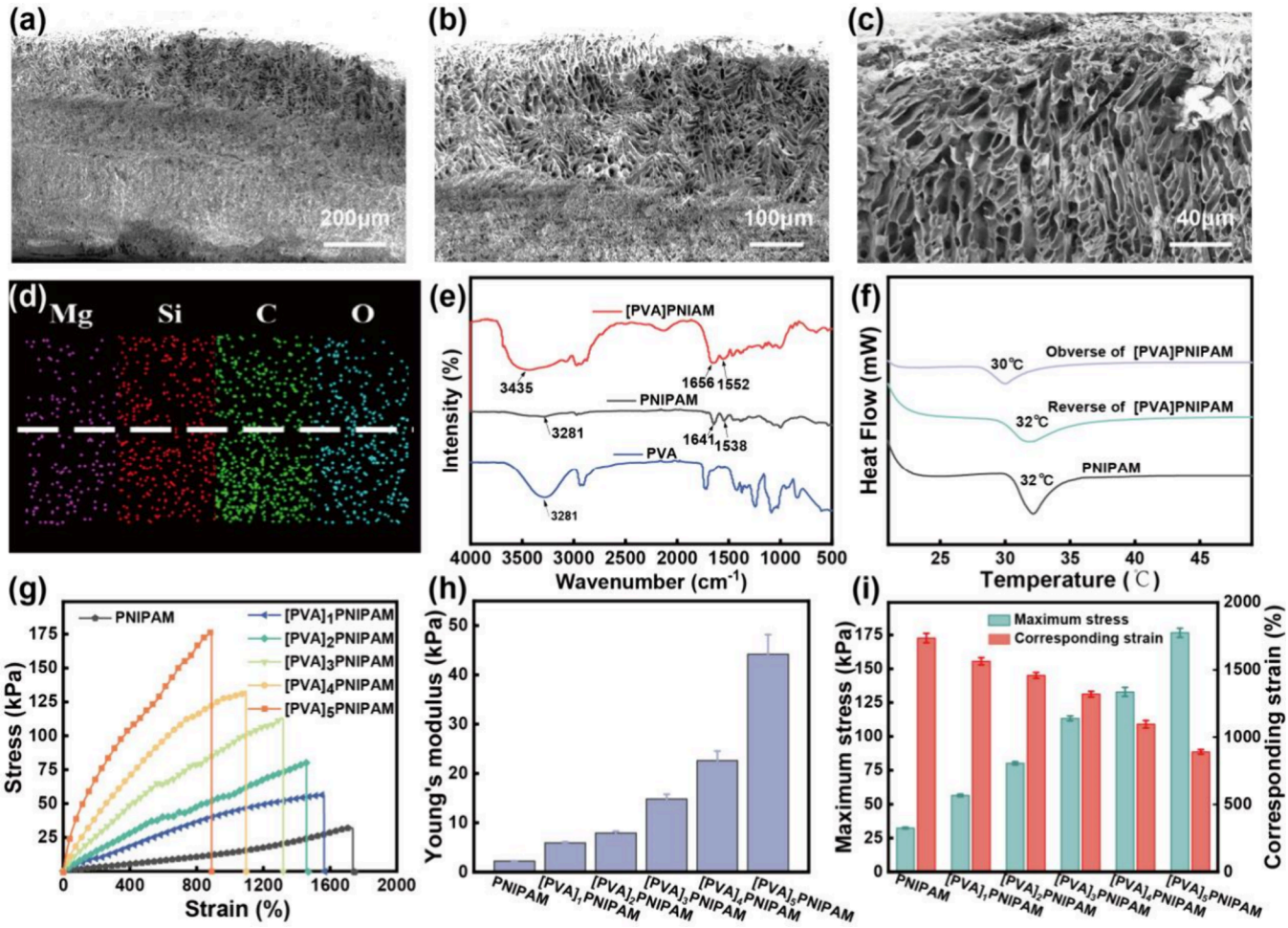

Figure 2. (a–c) Scanning electron microscopy (SEM) images of $[PVA]_3$PNIPAM hydrogels with different magnifications: (a) overall cross-section, (b) heterogeneous junction structure, and (c) corresponding local pore structures. (d) Corresponding mapping of the O, C, Si, Mg elements in the cross-section of the freeze-dried $[PVA]_3$PNIPAM hydrogel. (e) FTIR spectra of PVA polymer membrane and PNIPAM and $[PVA]_3$PNIPAM hydrogels. (f) DSC curves of PNIPAM and obverse and reverse parts of $[PVA]_3$PNIPAM hydrogels. (g–i) Mechanical property of pure PNIPAM and $[PVA]_x$PNIPAM hydrogels obtained at different diffusion times: (g) tensile stress–strain curves, (h) Young's modulus, (i) maximun stress and corresponding strain. The error bars of the stress–strain curves are the standard deviations calculated from eight data.

curve, focusing on the strain range from 0 to 100%. To ensure statistical reliability of the results, a minimum of five samples were tested under each set of experimental conditions.

To assess the actuation capabilities of hydrogel-based actuators, an experimental setup was established involving two glass jars filled with deionized water, one maintained at a cool temperature of 20 °C and the other at a warm temperature of 50 °C. Hydrogels were prepared into strips (40 mm × 10 mm). For the testing procedure, one end of a strip was fixed by using a clamp along its longer dimension, leaving the opposite end to hang freely. These strips were then individually submerged in the warmer water, causing them to bend toward the hydrogel side as a reaction to the elevated temperature. After each strip achieved its peak bending angle, it was swiftly moved to the cooler water for its original shape restoration. The entire actuation cycle was captured on a digital camera, with specific moments frozen in screenshots for subsequent analysis. The bending angles at various intervals were quantified using ImageJ software, following a methodology that calculates the central angle of deformation, a technique well-documented in prior research (Figure S1).[34] The bending amplitude was defined as the variance between the maximum and initial bending angles, and the bending velocity was derived from the change in the angle over the measured time frame. To attest to the

https://doi.org/10.1021/acsapm.4c00536
ACS Appl. Polym. Mater. 2024, 6, 5890–5899

durability and repeatability of the hydrogel's actuation behavior, this bending−recovery cycle was conducted 20 times for each strip. Additionally, to ensure the consistency and reliability of the findings, the entire experiment was replicated five times for each hydrogel specimen.

3. RESULTS AND DISCUSSION

3.1. Design and Fabrication of Polymeric Membrane Diffusion-Induced Gradient Structured Hydrogel. PVA, an advanced polymer material, contains numerous alcohol groups and can form hydrogen bonds with water. This polymer is readily soluble in polar water and slightly soluble in organic solvents. Consequently, we initially prepared polyvinyl alcohol (PVA) polymer films employing an evaporation method. Subsequently, [PVA]PNIPAM hydrogels with gradient structures were prepared through the hydrolysis and diffusion of PVA films in water-soluble precursor solutions containing NIPAM monomers. As illustrated in Figure 1, the precursor solution comprises a homogeneous mixture of NIPAM monomer, cross-linker (Laponite XLG), and photoinitiator (Irg.184). This mixture is then injected into a mold consisting of a glass slide and silica gel (40 mm × 10 mm × 1 mm). The PVA polymer film extends across the surface of the aqueous mixture, facilitating its hydrolysis while maintaining a sealed environment and allowing the hydrolyzed PVA molecules to diffuse gradually downward in the solution. Delamination takes place at the interface between the diffuse and undiffused regions. UV-induced free radicals stabilize this heterogeneous porous structure, ultimately resulting in anisotropic hydrogels. Subsequently, the resulting hydrogel was immersed in an aqueous solution of glutaraldehyde for final fixation and cross-linking of PVA. Compared to pure PNIPAM, the weight of the hydrogel after drying increased upon the introduction of PVA, indicating successful incorporation of PVA into the PNIPAM hydrogel (Figure S2). Moreover, $[PVA]_x$PNIPAM hydrogels with varying hydrolysis diffusion times exhibit similar weights after drying, as glutaraldehyde can cross-link PVA, allowing for the retention of incompletely hydrolyzed PVA on the hydrogels.

The [PVA]PNIPAM composite hydrogel, induced by hydrolytic diffusion of the PVA polymer film, exhibits a heterogeneous gradient porous network structure (Figure 2a−c). Pores near the top of the PVA film are large and sparse, whereas those at the bottom are small and dense. An evident dividing line exists between these two regions. Pure PNIPAM hydrogel, which shrinks in volume in hot water, exhibits isotropic characteristics and a uniform porous network structure in SEM (Figure S3). Following an extended hydrolysis−diffusion process, PVA is evenly dispersed in the solution, resulting in a hydrogel with a uniform porous network structure (Figure S4). We hypothesize that the inhomogeneous hydrogel structure results from the thermal motion of molecules during the hydrolysis of the PVA film on the surface of the precursor solution. This process leads to PVA molecules occupying the positions of NIPAM monomers in the precursor solution. Consequently, during the UV-induced NIPAM polymerization process, a multiphase porous gradient structure forms, featuring sparse macropores at the top and dense micropores at the bottom. Elemental map analysis (Figure 2d) reveals that the concentrations of C, O, Mg, and Si are lower at the top than at the bottom. This observation aligns with our hypothesis that a greater number of PVA molecules at the top layer of NIPAM monomers leads to reduced cross-linking of NIPAM with the nanoclay Laponite. The decreased cross-linking is evidenced by the lower distribution of C, O, Mg, and Si elements. Additionally, FTIR spectroscopy analyses were conducted on PVA films, pure PNIPAM hydrogels, and [PVA]PNIPAM hydrogels (Figure 2e). The absorption peaks of pure PNIPAM hydrogel, at approximately 1641 and 1538 cm^{-1}, correspond to the amides I (C═O) and II ($-NH_2$) bands in PNIPAM.[41] In the FTIR spectrum of the [PVA]PNIPAM gradient structure hydrogel after PVA hydrolysis and diffusion, the C═O stretching vibration peak shifted from 1641 cm^{-1} and the $-NH_2$ bending vibration peak moved from 1538 to 1552 cm^{-1}. Both PNIPAM hydrogel and PVA film exhibit characteristic peaks near 3281 cm^{-1}, corresponding to the N−H stretching vibration in PNIPAM's amide group and the −OH stretching vibration in the PVA film. However, in the [PVA]PNIPAM hydrogel, this peak shifts to approximately 3435 cm^{-1}. This shift is attributable to the enhanced hydrogen bonding interaction between the hydroxyl groups of PVA and the C═O of PNIPAM's amide bond following PVA hydrolysis and diffusion. Simultaneously, this interaction impedes the binding of $-NH_2$ to C═O in PNIPAM, enhancing the compatibility between PNIPAM and PVA within the hydrogel.[46] DSC test results (Figure 2f) indicate that the phase transition temperature (LCST) of the temperature-sensitive PNIPAM hydrogel is approximately 32 °C. Below the LCST, the hydroxyl groups of PNIPAM form hydrogen bonds with its amide groups, resulting in PNIPAM being in a swollen state in water. When the temperature exceeds the LCST, the enhanced hydrophobic effect of the isopropyl group leads to the dehydration of the hydrophilic amide group. This causes the PNIPAM chain to undergo a conformational change from a loose nematic to a tight spherical structure, resulting in volume shrinkage.[47−49] The introduction of PVA resulted in a decrease of the LCST to 30 °C at the top of the [PVA]PNIPAM hydrogel, while it remained at 32 °C at the bottom. This change can be attributed to the strong hydrogen bonds formed between PNIPAM and PVA. The interaction between PVA's hydroxyl group and C═O prevents the binding of $-NH_2$ to C═O, rendering the resulting amide group unstable. Consequently, hydrophobic interactions dominate, leading to the observed decrease in the LCST at the top of the hydrogel. Concurrently, the introduction of PVA significantly affects the mechanical properties of the hydrogel.

The maximum strain of the pure PNIPAM hydrogel reaches 1735%, while its maximum stress is only 32 kPa and the Young's modulus stands at 2.23 kPa (Figure 2g−i). These values highlight the inherent limitations of pure PNIPAM hydrogels in terms of their load-bearing capacity and structural rigidity. In contrast, the Young's modulus of the [PVA]-PNIPAM hydrogel progressively increased with the hydrolysis duration of the PVA membrane (Figure 2h). This increase is attributed to the added PVA promoting hydrogen bonding within the top diffusion layer of the hydrogel, leading to the formation of a secondary network and increased stiffness throughout the hydrogel network. Notably, at a hydrolysis duration of 120 min, the $[PVA]_5$PNIPAM hydrogel's maximum stress reached 176 kPa (Figure 2i) and its Young's modulus attained 44.19 kPa (Figure 2h). These values are 5.5 and 20 times higher, respectively, compared with those of the pure PNIPAM hydrogel. The significant improvement in mechanical properties highlights that the addition of PVA effectively alters the structural properties of the hydrogel, and

https://doi.org/10.1021/acsapm.4c00536
ACS Appl. Polym. Mater. 2024, 6, 5890−5899

the increased strength and stiffness make [PVA]PNIPAM hydrogels more suitable for applications requiring higher mechanical elasticity.

3.2. Temperature-Responsive Driving Behavior of [PVA]PNIPAM Gradient Hydrogels. It is well-established that PNIPAM expels water from its hydrated state and undergoes volume shrinkage when the temperature exceeds the LCST. In contrast, when the temperature drops below the LCST, PNIPAM hydrogels absorb water from the environment, resulting in volume expansion (Figure 4a1). As a result, hydrogels composed solely of PNIPAM, which are characterized by their uniform structure, undergo a reduction in volume but do not exhibit any bending when submerged in water at a temperature of 50 °C (Figure 3a). However,

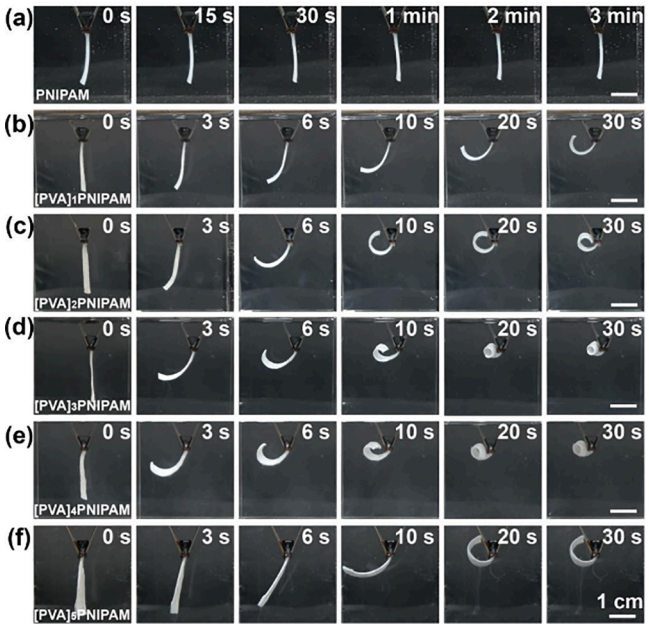

Figure 3. Optical photographs of the bending process of (a) pure PNIPAM, (b) $[PVA]_1$PNIPAM, (c) $[PVA]_2$PNIPAM, (d) $[PVA]_3$PNIPAM, (e) $[PVA]_4$PNIPAM, and (f) $[PVA]_5$PNIPAM hydrogel with a thickness of 1 mm in water at 50 °C.

hydrogels that combine poly(vinyl alcohol) (PVA) with PNIPAM, benefiting from a gradient in pore size, are capable of demonstrating dynamic bending responses when exposed to water at the same temperature of 50 °C (Figure 3b–f). This observation confirms the significant role of gradient microstructure in the responsive actuation behavior of hydrogel actuators. In the [PVA]PNIPAM hydrogel, the diffusion and nondiffusion layers exhibit significant differences in network pore size, hydrogen bond interaction, and phase transition temperature. As shown in Figure S5, the addition of PVA to the PNIPAM hydrogel results in the formation of a strong hydrogen bond between the hydroxyl group of PVA and the amide group of PNIPAM, thereby impeding the binding of $-NH_2$ and C═O in PNIPAM.[50] The incorporation of PVA enhances the mechanical properties of the PNIPAM hydrogel; however, due to PVA's lack of thermal response, its introduction leads to a reduction in the thermal response of the hydrogel. Consequently, in the diffusion region, the presence of PVA results in a lesser volume contraction, whereas the nondiffusion region experiences a greater volume contraction.

This results in uneven volume shrinkage during the actuation process. This uneven volume shrinkage induces internal stress between the top diffusion layer and the bottom nondiffusion layer of the hydrogel. This stress acts as a driving force for the deformation and recovery of the [PVA]PNIPAM hydrogel, leading to pronounced bending behavior in the lateral nondiffusion zone (Figure 4a2). The distinct behaviors of these layers underpin the hydrogel's unique actuation capabilities, illustrating the crucial role of structural design in dictating the material's functional properties. For example, when placed in hot water, the $[PVA]_1$PNIPAM hydrogel achieved a maximum bending angle of 210.4° within 30 s (Figure 3b). The SEM image (Figure S6a) of the $[PVA]_1$PNIPAM hydrogel's surface reveals that with only 10 min of diffusion time, the PVA is minimally hydrolyzed, covering the pores on the hydrogel's surface. This impedes water's entry and exit at the top. Consequently, the pore-rich bottom, with its larger specific surface area, generates a greater cohesive force than the top, resulting in the hydrogel bending toward the bottom. In addition, submerging $[PVA]_1$PNIPAM hydrogels in cold water at 25 °C enables rapid recovery within 20 s (Figure S7a). As the hydrolytic diffusion time of the PVA film increases, the PVA-covered surface area gradually decreases (Figure S6b–e), and the thickness of the diffusion layer becomes more pronounced (Figure S8). Notably, with the hydrolytic diffusion time extended to 30 min, the $[PVA]_3$PNIPAM hydrogels could rapidly bend within 30 s, achieving a maximum bending angle of 527.3° (Figure 3d). This behavior is attributed to a more distinct separation between the diffusion and nondiffusion layers, a larger disparity in volume shrinkage, and an increase in both driving speed and bending angle. Specifically, the volume shrinkage ratio of the nondiffusing layer in the $[PVA]_x$PNIPAM hydrogel is higher than that of the diffusing layer, resulting in the hydrogel bending more rapidly toward the nondiffusing layer. These findings highlight the critical role of hydrolytic diffusion time in modulating the mechanical and responsive properties of gradient hydrogels.

As depicted in Figure 4b, the bending angle–time curve of the hydrogel is linear during the initial 15 s. As the hydrolysis diffusion time increases, the bending rate of the $[PVA]_x$PNIPAM hydrogel nearly doubles, with the maximum bending rate observed in the $[PVA]_3$PNIPAM hydrogel reaching 30.4° per second (Figure 4c). The increased rate of bending also indicates the sensitivity of the hydrogel to hot water. Hydrogels with higher sensitivity demonstrate improved thermal responsiveness, evident in faster bending rates and larger bending angles. The $[PVA]_3$PNIPAM hydrogel exhibited the highest sensitivity with an increasing hydrolysis diffusion time. Additionally, it was observed that the actuation performance of hydrogels without GA cross-linking was markedly diminished (Figure S9). This phenomenon may be attributed to the hydrophobic nature of PVA after GA cross-linking, resulting from aldehyde group condensation, thereby further diminishing the thermal response in the diffusion region. This disparity accentuates the difference in volume shrinkage between the diffusion region and the nondiffusion region. Additionally, the larger bending angle and the friction generated by bending mean that more time is required for the hydrogel to absorb water and return to its initial state in cold water (Figure S7). When the hydrolysis time of the PVA film was extended to 60 min, the response rate of the $[PVA]_4$PNIPAM hydrogel in hot water began to decrease.

https://doi.org/10.1021/acsapm.4c00536
ACS Appl. Polym. Mater. 2024, 6, 5890–5899

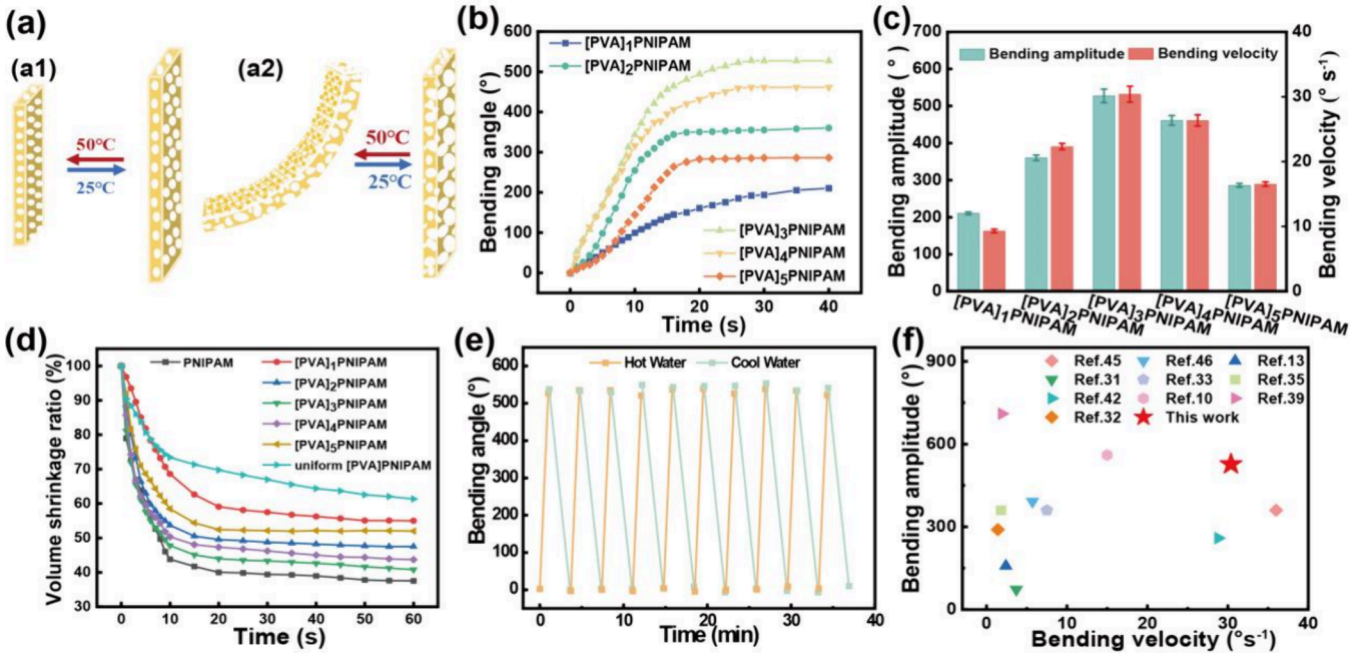

Figure 4. (a) Schematic illustration of the temperature-responsive bending mechanism of the $[PVA]_x$PNIPAM (x = 1, 2, 3, 4, 5) hydrogel. (b) Relationship between the bending angle and time of different $[PVA]_x$PNIPAM (x = 1, 2, 3, 4, 5) hydrogel in hot water. (c) Overall bending amplitude and the initial bending velocity during the first 15 s of different $[PVA]_x$PNIPAM (x = 1, 2, 3, 4, 5) hydrogel in hot water. (d) Volume shrinkage ratio of $[PVA]_x$PNIPAM (x = 1, 2, 3, 4, 5) hydrogel in hot water. (e) Relationship between the bending angle, response time, and recovery time of the $[PVA]_3$PNIPAM hydrogel in response to temperature change for six cycles. (f) Comparison of bending amplitude and responding time of different hydrogel actuators in different environments.

The maximum bending angle reached 461° within 30 s, and the maximum bending rate decreased to 26.3° per second (Figure 4c). Continuing to extend the hydrolytic diffusion time of the PVA film, the $[PVA]_5$PNIPAM hydrogel exhibited a maximum bending angle of only 286°, with a bending rate of 16.5° per second (Figure 4c). Collectively, the bending rate and bending angles of $[PVA]_x$PNIPAM hydrogels collectively exhibit a pattern of an initial increase followed by a decrease as hydrolysis time increases. This phenomenon can be attributed to the increased hydrolysis time, resulting in larger pore sizes, which in turn reduces the specific surface area in contact with the external water environment. Consequently, the outflow channel for free water diminishes, resulting in lower water flow and outflow rates. This deceleration in volume contraction leads to an increasing disparity in volume change between the diffusion and nondiffusion layers. This increase in combined force enhances the driving rate. With further increases in hydrolysis diffusion time, the pore size in the diffusion layer tends to stabilize, and the increase in thickness results in increased resistance, opposing the direction of deformation. Meanwhile, a decrease in the thickness of the nondiffusion layer results in reduced driving force, aligned with the direction of deformation, thereby diminishing the combined force and gradually decreasing the driving rate. This also provides a logical explanation for the hydrogel's rate of water loss (Figure 4d). Additionally, experimental results indicate that the thicknesses of the PVA film and the PNIPAM hydrogel significantly influence the overall architecture, volume contraction, and bending behavior of the anisotropic hydrogel. As depicted in Figure S10, increasing the thickness of the PVA film (from 10 to 50 μm) results in a driving performance that initially accelerates and then slows down. Further analysis reveals that, under the same hydrolysis diffusion time, a thinner PVA film yields a less thick diffusion layer per unit time. Conversely, an excessively thick PVA film cannot be fully hydrolyzed within the corresponding time frame, leading to surface pores remaining covered by the PVA film, which hinders water loss from the hydrogel. PVA films that are either too thin or too thick result in a smaller difference in volumetric shrinkage between the diffused and nondiffused layers, reduced deformation forces, and slower bending speeds. Similarly, fixing the PVA film thickness and diffusion time and increasing the hydrogel thickness (from 1 to 3 mm), the driving speed of the [PVA]PNIPAM hydrogel decreases due to the increased overall thickness and gravity of the hydrogel, exhibiting a gradual declining trend (Figure S11). Upon comprehensive analysis of how PVA film hydrolysis time, PVA film thickness, and overall hydrogel thickness influence the driving rate, we determined that the $[PVA]_3$PNIPAM gradient structure hydrogel, induced by hydrolysis and diffusion of a 30 μm thick PVA film for 30 min, exhibits the best driving performance. Compared to previously reported hydrogel-driven materials, it shows significant enhancements in both the maximum bending angle and maximum bending rate (Figure 4f). Repeated thermal response bending-recovery experiments were conducted on the $[PVA]_3$PNIPAM hydrogel (Figure 4e). The experimental results indicated that there were no significant changes in the bending rate, response time, or recovery time of the gradient structure hydrogel, demonstrating its excellent actuation repeatability, reversibility, and practicality. These findings underscore the superiority of the [PVA] PNIPAM hydrogel in terms of performance and reliability, marking a notable advancement in the field of hydrogel-driven materials.

3.3. [PVA]PNIPAM Gradient Hydrogel as a Soft Actuator for Programmable Deformation Applications.

https://doi.org/10.1021/acsapm.4c00536
ACS Appl. Polym. Mater. 2024, 6, 5890−5899

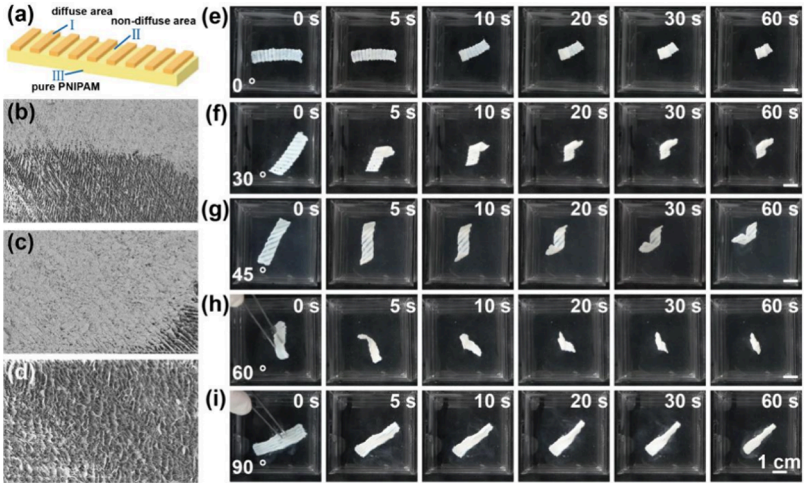

Figure 5. Controllable actuation of stripe-patterned heterogeneous $[PVA]_3$PNIPAM hydrogel actuators in response to a temperature change. The stripe width was 2 mm with the fringe spacing of 1 mm. (a) Schematic diagram of striped pattern $[PVA]_3$PNIPAM hydrogel preparation, taking 0° as an example. (b–d) SEM images of different parts of the stripe-patterned $[PVA]_3$PNIPAM hydrogel strip with orientation angle of 0°. (e–i) The stripes were oriented at different angles relative to the length direction of the hydrogel strip: (e) 0°, (f) 30°, (g) 45°, (h) 60°, and (i) 90°.

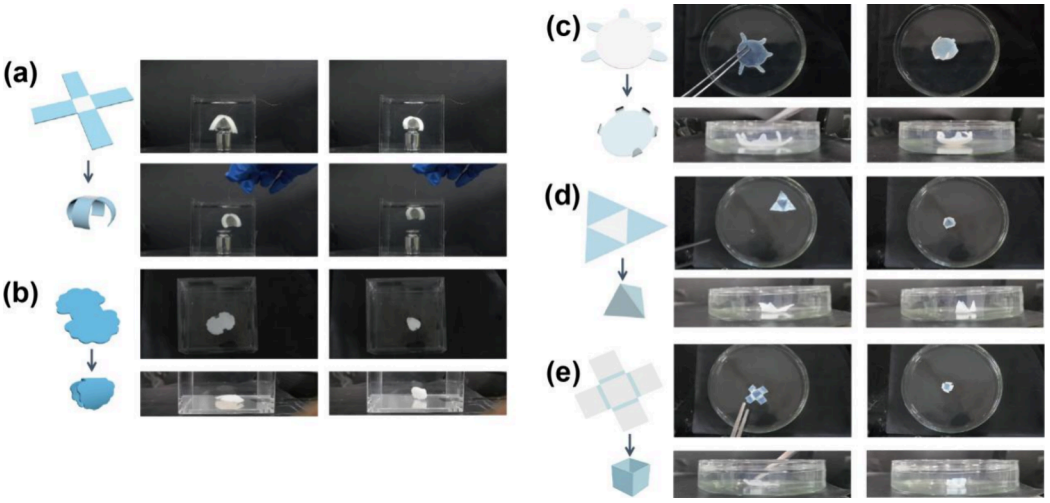

Figure 6. Controllable deformation of heterogeneous $[PVA]_3$PNIPAM hydrogels in response to temperature change. (a) Capture and transportation of a cuvette lid by a cross-shaped hydrogel as the gripper. (b) Bionic shell inverted in hot water. (c) The bionic turtle curls its limbs in hot water. (d) Closure of the tetrahedral hydrogel actuator in hot water. (e) Closure of the box type hydrogel actuator in hot water.

Given the superior response characteristics and mechanical properties of $[PVA]_3$PNIPAM hydrogels, we engineered a PVA film with stripe patterning to create [PVA]PNIPAM hydrogel actuators capable of helical bending. As illustrated in Figure 5a, the mask template and polymer film were sequentially positioned on the hydrogel precursor's surface, and the mask template was removed after UV-induced polymerization. The orientation angle θ is defined as the angle between the alignment direction of the striped PVA film and the long axis of the hydrogel. Region "I" is the diffuse area, while region "II" is the nondiffuse area covered by the mask plate. SEM surface topography confirmed the interleaved diffuse/nondiffuse structure (Figure 5b), the surface of the diffuse region covered by the PVA film (Figure 5c), and the nondiffuse region's surface uniformly populated with small pores (Figure 5d). The selective hydrolytic diffusion's effect on the hydrogel's microstructure consequently influences its stimuli-responsive behavior. Figure 5e–i demonstrates that hydrogels with different stripe orientation angles undergo corresponding helical changes upon thermal stimulation in hot water. Pores obstructed by the PVA film impeded water exchange to a degree, whereas the bottom, with its larger specific surface area and higher volume shrinkage, caused the stripe-programmed hydrogels to bend toward the nondiffusive region, aligning with the previously observed pattern. Furthermore, the variation in cohesion resulting from differential volume shrinkage induces the hydrogel to curl helically in a direction perpendicular to the stripes, oriented along the axis of the stripe orientation. This innovative approach not only showcases the potential for precise control over hydrogel properties but also opens up possibilities for the design of advanced hydrogel-based actuators with tailored response behaviors.

Drawing on insights from the patterning effect on the hydrogel bending behavior, we have designed various 3D specialized deformations. For instance, we developed a four-armed hydrogel manipulator capable of grasping objects weighing approximately 600 mg in hot water at 50 °C (Figure

https://doi.org/10.1021/acsapm.4c00536
ACS Appl. Polym. Mater. 2024, 6, 5890–5899

6a). By differentially structuring the PVA film in distinct planar regions, we achieved both a curved shape and localized deformations. As depicted in Figure 6b, we designed a bionic shell that, upon stimulation, exhibits a bowl-like deformation of its curved surface. Concurrently, the shell can support its own weight upside down on a flat surface, which is attributed to its superior mechanical properties. In Figure 6c, we have fabricated a bionic turtle with a polymer film specifically applied to the limbs. This gradient structure on a flat surface is engineered to exhibit "stress behavior" upon stimulation, causing the limbs to roll the shell back. Expanding beyond the bending mechanism, we introduced a folding mechanism inspired by origami techniques. While the bending mechanism occurs on a continuous two-dimensional surface, the folding mechanism represents a one-dimensional sharp bend. This approach can also be interpreted as a gradient structural design along the thickness dimension. Based on this principle, we utilize this folding process to create complex 3D shapes, such as cubes and pyramids. As shown in Figure 6d,e, we induce hydrolytic diffusion of the polymer film in specific regions. In these specific regions, the hydrogel exhibits an anisotropic driving structure, in contrast to the other parts. When placed in hot water at 50 °C, the hydrogel sheets automatically fold in the predetermined direction, ultimately forming an open cubic box and a pyramid. This automatic folding behavior not only exemplifies the adaptability of hydrogels but also opens up avenues for creating self-assembling structures in the field of material science.

4. CONCLUSION

Inspired by the molecular thermal diffusion phenomenon, we have successfully developed gradient porous hydrogel actuators, characterized by rapid actuation and robust mechanical properties, through a straightforward diffusion technique. The water-soluble polymer film, PVA, undergoes gradual hydrolysis and diffusion on the surface of the hydrogel monomer precursor solution. Ultraviolet light induces cross-linking and enhances this interaction, resulting in the formation of anisotropic hydrogels with varying microstructures. By meticulously controlling the amount of the polymer film and the volume of the hydrogel precursor solution along with the duration of hydrolysis and diffusion between these components, anisotropic hydrogels with precisely tailored microstructures were successfully fabricated. These hydrogel actuators exhibit rapid responsiveness to temperature stimuli and maintain a stable operation under repeated temperature stimuli. Furthermore, we have explored both shape and thickness gradients in the polymer film design to achieve localized, folded, and curved deformations in the hydrogel actuator. This innovative approach not only streamlines the fabrication of various responsive hydrogels with programmable multifunctionality but also expands the scope of their applications in soft robotics, smart sensing, and human–machine interface materials.

■ ASSOCIATED CONTENT

Data Availability Statement

Data will be made available on request.

Supporting Information

The Supporting Information is available free of charge at https://pubs.acs.org/doi/10.1021/acsapm.4c00536.

Schematic measurement for bending angle of the [PVA]PNIPAM hydrogel actuators; weight of pure PNIPAM hydrogel and [PVA]PNIPAM hydrogel with different hydrolysis diffusion time after drying; cross-section SEM of pure PNIPAM hydrogel and uniform [PVA]PNIPAM hydrogel; schematic diagram of the hydrogen bond formed between PVA and PNIPAM; surface SEM images of $[PVA]_x$PNIPAM hydrogels and PNIPAM hydrogel; optical photographs of the bending process of [PVA]PNIPAM hydrogel with or without GA cross-linking; optical photographs of the recovering process of $[PVA]_x$PNIPAM hydrogel; cross-section SEM images of [PVA]PNIPAM hydrogels at different diffusion times; effect of PVA films thickness on [PVA]PNIPAM hydrogel actuator; effect of hydrogel thickness on [PVA]PNIPAM hydrogel actuator (PDF)

■ AUTHOR INFORMATION

Corresponding Authors

Lin Cheng − *Key Laboratory of Optical Field Manipulation of Zhejiang Province, School of Science, Zhejiang Sci-Tech University, Hangzhou 310018, China;* orcid.org/0000-0001-8680-1383; Email: chenglin@zstu.edu.cn

Huaping Wu − *Key Laboratory of Special Purpose Equipment and Advanced Processing Technology, Ministry of Education and Zhejiang Province, College of Mechanical Engineering, Zhejiang University of Technology, Hangzhou 310023, China;* orcid.org/0000-0003-4505-7062; Email: wuhuaping@gmail.com

Aiping Liu − *Key Laboratory of Optical Field Manipulation of Zhejiang Province, School of Science, Zhejiang Sci-Tech University, Hangzhou 310018, China;* orcid.org/0000-0002-2338-062X; Email: liuaiping1979@gmail.com

Authors

Ruofei Wang − *Key Laboratory of Optical Field Manipulation of Zhejiang Province, School of Science, Zhejiang Sci-Tech University, Hangzhou 310018, China*

Chengnan Qian − *Key Laboratory of Optical Field Manipulation of Zhejiang Province, School of Science, Zhejiang Sci-Tech University, Hangzhou 310018, China*

Complete contact information is available at: https://pubs.acs.org/10.1021/acsapm.4c00536

Author Contributions

Ruofei Wang: investigation, writing—original draft, conceptualization, methodology, formal analysis. Lin Cheng: supervision, project administration, writing—review and editing. Chengnan Qian: investigation. Huaping Wu: project administration. Aiping Liu: supervision, funding acquisition, writing—review and editing.

Notes

The authors declare no competing financial interest.

■ ACKNOWLEDGMENTS

This work was supported by the National Natural Science Foundation of China (Grants 12272351, 2372168, and 11972323), the Youth Top-notch Talent Project of Zhejiang Ten Thousand Plan of China (Grant ZJWR0308010), the Zhejiang Provincial Natural Science Foundation of China (Grants Z24A020008 and LR20A020002), and the "Pioneer"

and "Leading Goose" R&D Program of Zhejiang (Grant 2023C01051).

REFERENCES

(1) Yao, C.; Liu, Z.; Yang, C.; Wang, W.; Ju, X.-J.; Xie, R.; Chu, L.-Y. Poly (N-isopropylacrylamide)-clay nanocomposite hydrogels with responsive bending property as temperature-controlled manipulators. *Adv. Funct. Mater.* **2015**, *25*, 2980−91.
(2) Lin, H.; Ma, S.; Yu, B.; Pei, X.; Cai, M.; Zheng, Z.; Zhou, F.; Liu, W. Simultaneous surface covalent bonding and radical polymerization for constructing robust soft actuators with fast underwater response. *Chem. Mater.* **2019**, *31*, 9504−12.
(3) Liu, K.; Zhang, Y.; Cao, H.; Liu, H.; Geng, Y.; Yuan, W.; Zhou, J.; Wu, Z.; Shan, G.; Bao, Y.; Zhao, Q.; Xie, T.; Pan, P. Programmable reversible shape transformation of hydrogels based on transient structural anisotropy. *Adv. Mater.* **2020**, *32*, 2001693.
(4) Fuhrer, R.; Athanassiou, E. K.; Luechinger, N. A.; Stark, W. J. Crosslinking metal nanoparticles into the polymer backbone of hydrogels enables preparation of soft, magnetic field-driven actuators with muscle-like flexibility. *Small.* **2009**, *5*, 383−8.
(5) Gao, F.; Zhang, N.; Fang, X.; Ma, M. Magnetically directed soft actuators driven by moisture. *J. Mater. Chem. C* **2017**, *5*, 4129−33.
(6) Cheng, R.; Zhu, L.; Huang, W.; Mao, L.; Zhao, Y. Dynamic scaling of ferromagnetic micro-rod clusters under a weak magnetic field. *Soft Matter.* **2016**, *12*, 8440−7.
(7) Osada, Y.; Okuzaki, H.; Hori, H. A polymer gel with electrically driven motility. *Nature.* **1992**, *355*, 242−4.
(8) Xue, B.; Qin, M.; Wang, T.; Wu, J.; Luo, D.; Jiang, Q.; Li, Y.; Cao, Y.; Wang, W. Electrically controllable actuators based on supramolecular peptide hydrogels. *Adv. Funct. Mater.* **2016**, *26*, 9053−62.
(9) Li, Q.; Wang, X.; Dong, L.; Liu, C.; Fan, S. Spirally deformable soft actuators and their designable helical actuations based on a highly oriented carbon nanotube film. *Soft Matter.* **2019**, *15*, 9788−96.
(10) Pourmadadi, M.; Ahmadi, M.; Yazdian, F. Synthesis of a novel pH-responsive Fe3O4/chitosan/agarose double nanoemulsion as a promising Nanocarrier with sustained release of curcumin to treat MCF-7 cell line. *Int. J. Biol. Macromol.* **2023**, *235*, 123786.
(11) Li, Z.; Liu, P.; Ji, X.; Gong, J.; Hu, Y.; Wu, W.; Wang, X.; Peng, H.-Q.; Kwok, R. T. K.; Lam, J. W. Y.; Lu, J.; Tang, B. Z. Bioinspired simultaneous changes in fluorescence color, brightness, and shape of hydrogels enabled by AIEgens. *Adv. Mater.* **2020**, *32*, 1906493.
(12) Zheng, C.; Jin, F.; Zhao, Y.; Zheng, M.; Liu, J.; Dong, X.; Xiong, Z.; Xia, Y.; Duan, X. Light-driven micron-scale 3D hydrogel actuator produced by two-photon polymerization microfabrication. *Sens. Actuators B: Chem.* **2020**, *304*, 127345.
(13) Ma, C.; Lu, W.; Yang, X.; He, J.; Le, X.; Wang, L.; Zhang, J.; Serpe, M. J.; Huang, Y.; Chen, T. Bioinspired anisotropic hydrogel actuators with on-off switchable and color-tunable fluorescence behaviors. *Adv. Funct. Mater.* **2018**, *28*, 1704568.
(14) Ni, C.; Chen, D.; Wen, X.; Jin, B.; He, Y.; Xie, T.; Zhao, Q. High speed underwater hydrogel robots with programmable motions powered by light. *Nat. Commun.* **2023**, *14*, 7672.
(15) Zheng, S. Y.; Shen, Y.; Zhu, F.; Yin, J.; Qian, J.; Fu, J.; Wu, Z. L.; Zheng, Q. Programmed deformations of 3D-Printed tough physical hydrogels with high response speed and large output force. *Adv. Funct. Mater.* **2018**, *28*, 1803366.
(16) Li, T.; Wei, H.; Zhang, Y.; Wan, T.; Cui, D.; Zhao, S.; Zhang, T.; Ji, Y.; Algadi, H.; Guo, Z.; Chu, L.; Cheng, B. Sodium alginate reinforced polyacrylamide/xanthan gum double network ionic hydrogels for stress sensing and self-powered wearable device applications. *Carbohyd. Polym.* **2023**, *309*, 120678.
(17) Shi, Q.; Liu, H.; Tang, D.; Li, Y.; Li, X. J.; Xu, F. Bioactuators based on stimulus-responsive hydrogels and their emerging biomedical applications. *NPG Asia Mater.* **2019**, *11*, 64.
(18) Zhang, H.; Ma, Y.; Wang, Y.; Niu, L.; Zou, R.; Zhang, M.; Liu, H.; Genin, G. M.; Li, A.; Xu, F. Rational design of soft-hard interfaces through bioinspired engineering. *Small* **2023**, *19*, 2204498.
(19) Shin, S. R.; Migliori, B.; Miccoli, B.; Li, Y.-C.; Mostafalu, P.; Seo, J.; Mandla, S.; Enrico, A.; Antona, S.; Sabarish, R.; Zheng, T.; Pirrami, L.; Khademhosseini, A.; et al. Electrically driven microengineered bioinspired soft robots. *Adv. Mater.* **2018**, *30*, 1704189.
(20) Calvert, P. Hydrogels for soft machines. *Adv. Mater.* **2009**, *21*, 743−56.
(21) Zheng, W. J.; An, N.; Yang, J. H.; Zhou, J.; Chen, Y. M. Tough Al-alginate/poly(N-isopropylacrylamide) hydrogel with tunable LCST for soft robotics. *ACS Appl. Mater. Interfaces* **2015**, *7*, 1758−64.
(22) Tao, N.; Zhang, D.; Li, X.; Lou, D.; Sun, X.; Wei, C.; Li, J.; Yang, J.; Liu, Y. N. Near-infrared light-responsive hydrogels via peroxide-decorated MXene-initiated polymerization. *Chem. Sci.* **2019**, *10*, 10765−71.
(23) Kuang, Z.; Xu, W.; Li, J.; Fan, Z.; Wang, R.; Ji, S.; Qian, C.; Cheng, L.; Wu, H.; Liu, A. Anisotropic aerogel induced gelatin hydrogel actuator with favourable mechanical properties and multiple solvent responsiveness. *Sens. Actuators B: Chem.* **2023**, *390*, 133932.
(24) Han, Z.; Wang, P.; Mao, G.; Yin, T.; Zhong, D.; Yiming, B.; Hu, X.; Jia, Z.; Nian, G.; Qu, S.; Yang, W. Dual pH-responsive hydrogel actuator for lipophilic drug delivery. *ACS Appl. Mater. Interfaces* **2020**, *12*, 12010−7.
(25) Kim, J.; Park, J.; Ahn, S.; Park, S.; Yu, H.; Yu, J.; Kim, D.; Lim, J. Y.; Hyun, K. A.; Koh, W. G.; Jung, H.-I. On-demand delivery of therapeutic extracellular vesicles by encapsulating in monodispersed photodegradable hydrogel microparticles using a droplet microfluidic device. *Sens. Actuators, B* **2023**, *394*, 134396.
(26) Qiu, Y.; Wang, C.; Lu, X.; Wu, H.; Ma, X.; Hu, J.; Qi, H.; Tian, Y.; Zhang, Z.; Bao, G.; Chai, H.; Song, J.; Liu, A. A biomimetic drosera capensis with adaptive decision-predation behavior based on multifunctional sensing and fast actuating capability. *Adv. Funct. Mater.* **2022**, *32*, 32.
(27) Peng, H.-Y.; Wang, W.; Gao, F.; Lin, S.; Liu, L.-Y.; Pu, X.-Q.; Liu, Z.; Ju, X.-J.; Xie, R.; Chu, L.-Y. Ultrasensitive diffraction gratings based on smart hydrogels for highly selective and rapid detection of trace heavy metal ions. *J. Mater. Chem. C* **2018**, *6*, 11356−67.
(28) Wang, Z.; Zhou, H.; Chen, W.; Li, Q.; Yan, B.; Jin, X.; Ma, A.; Liu, H.; Zhao, W. Dually synergetic network hydrogels with integrated mechanical stretchability, thermal responsiveness, and electrical conductivity for strain sensors and temperature alertors. *ACS Appl. Mater. Interfaces* **2018**, *10*, 14045−54.
(29) Ruan, D.; Chen, G.; Luo, X.; Cheng, L.; Wu, H.; Liu, A. Bionic octopus-like flexible three-dimensional force sensor for meticulous handwriting recognition in human-computer interactions. *Nano Energy* **2024**, *123*, 109357.
(30) Han, F.; Xie, X.; Wang, T.; Cao, C.; Li, J.; Sun, T.; Liu, H.; Geng, S.; Wei, Z.; Li, J.; Xu, F. Wearable hydrogel-based epidermal sensor with thermal compatibility and long term stability for smart colorimetric multi-signals monitoring. *Adv. Healthcare Mater.* **2023**, *12*, 2201730.
(31) Wei, S.; Lu, W.; Le, X.; Ma, C.; Lin, H.; Wu, B.; Zhang, P. J.; Theato, P. P.; Chen, P. T. Bioinspired synergistic fluorescence-color-switchable polymeric hydrogel actuators. *Angew. Chem., Int. Ed.* **2019**, *58*, 16243−51.
(32) Tan, Y.; Wang, D.; Xu, H.; Yang, Y.; An, W.; Yu, L.; Xiao, Z.; Xu, S. A fast, reversible, and robust gradient nanocomposite hydrogel actuator with water-promoted thermal response. *Macromol. Rapid Commun.* **2018**, *39*, 1700863.
(33) Liu, J.; He, S.; Liu, Z.; Wu, X.; Liu, J.; Shao, W. Novel multi-responsive soft actuator assembled with a graphene oxide nanoribbons doped strain hydrogel sensor with high sensitive and NIR-triggered performances. *Sens. Actuators B: Chem.* **2023**, *393*, 134217.
(34) Hua, L.; Xie, M.; Jian, Y.; Wu, B.; Chen, C.; Zhao, C. Multiple-responsive and amphibious hydrogel actuator based on asymmetric UCST-type volume phase transition. *ACS Appl. Mater. Interfaces* **2019**, *11*, 43641−8.
(35) Xu, W.; Dong, P.; Lin, S.; Kuang, Z.; Zhang, Z.; Wang, S.; Ye, F.; Cheng, L.; Wu, H.; Liu, A. Bioinspired bilayer hydrogel-based actuator with rapidly bidirectional actuation, programmable deforma-

https://doi.org/10.1021/acsapm.4c00536
ACS Appl. Polym. Mater. 2024, 6, 5890−5899

tion and devisable functionality. *Sens. Actuators B: Chem.* **2022**, *359*, 131547.
(36) Chen, Z.; Liu, J.; Chen, Y.; Zheng, X.; Liu, H.; Li, H. Multiple-stimuli-responsive and cellulose conductive ionic hydrogel for smart wearable devices and thermal actuators. *ACS Appl. Mater. Interfaces* **2021**, *13*, 1353−66.
(37) He, X.; Sun, Y.; Wu, J.; Wang, Y.; Chen, F.; Fan, P.; Zhong, M.; Xiao, S.; Zhang, D.; Yang, J.; Zheng, J. Dual-stimulus bilayer hydrogel actuators with rapid, reversible, bidirectional bending behaviors. *J. Mater. Chem. C* **2019**, *7*, 4970−80.
(38) Fan, W.; Shan, C.; Guo, H.; Sang, J.; Wang, R.; Zheng, R.; Sui, K.; Nie, Z. Dual- gradient enabled ultrafast biomimetic snapping of hydrogel materials. *Sci. Adv.* **2019**, *5*, No. eaav7174.
(39) Li, Y.; Liu, L.; Xu, H.; Cheng, Z.; Yan, J.; Xie, X.-M. Biomimetic gradient hydrogel actuators with ultrafast thermo-responsiveness and high strength. *ACS Appl. Mater. Interfaces* **2022**, *14*, 32541−50.
(40) Chen, Z.; Chen, Y.; Chen, C.; Zheng, X.; Li, H.; Liu, H. Dual-gradient PNIPAM-based hydrogel capable of rapid response and tunable actuation. *Chem. Eng. J.* **2021**, *424*, 130562.
(41) Tan, Y.; Wu, R.; Li, H.; Ren, W.; Du, J.; Xu, S.; Wang, J. Electric field-induced gradient strength in nanocomposite hydrogel through gradient crosslinking of clay. *J. Mater. Chem. B* **2015**, *3*, 4426−30.
(42) Liu, Y.; Takafuji, M.; Ihara, H.; Zhu, M.; Yang, M.; Gu, K.; Guo, W. Programmable responsive shaping behavior induced by visible multi-dimensional gradients of magnetic nanoparticles. *Soft. Matter.* **2012**, *8*, 3295−9.
(43) Tan, Y.; Wang, D.; Xu, H.; Yang, Y.; Wang, X.-L.; Tian, F.; Xu, P.; An, W.; Zhao, X.; Xu, S. Rapid recovery hydrogel actuators in air with bionic large-ranged gradient structure. *ACS Appl. Mater. Interfaces.* **2018**, *10*, 40125−31.
(44) Dong, P.; Xu, W.; Kuang, Z.; Yao, Y.; Zhang, Z.; Guo, D.; Wu, H.; Zhao, T.; Liu, A. Liquid stratification and diffusion-induced anisotropic hydrogel actuators with excellent thermosensitivity and programmable functionality. *Adv. Intell. Syst.* **2021**, *3*, 2100030.
(45) Li, Y.; Liu, L.; Xu, H.; Cheng, Z.; Yan, J.; Xie, X. M. Biomimetic gradient hydrogel actuators with ultrafast thermo-responsiveness and high strength. *ACS Appl. Mater. Interfaces* **2022**, *14*, 32541−32550.
(46) Schild, H. G.; Tirrell, D. A. Microcalorimetric detection of lower critical solution temperatures in aqueous polymer solutions. *J. Phys. Chem.* **1990**, *94*, 4352−4356.
(47) Ziolkowski, B.; Florea, L.; Theobald, J.; Benito-Lopez, F.; Diamond, D. Porous self-protonating spiropyran-based NIPAAm gels with improved reswelling kinetics. *J. Mater. Sci.* **2016**, *51*, 1392−9.
(48) Boutris, C.; Chatzi, E. G.; Kiparissides, C. Characterization of the LCST behaviour of aqueous poly(N-isopropylacrylamide) solutions by thermal and cloud point techniques. *Polymer.* **1997**, *38*, 2567−70.
(49) Gan, J.; Guan, X.; Zheng, J.; Guo, H.; Wu, K.; Liang, L.; Lu, M. Biodegradable, thermoresponsive PNIPAM-based hydrogel scaffolds for the sustained release of levofloxacin. *RSC Adv.* **2016**, *6*, 32967−78.
(50) Zhang, J.; Zheng, L.; Wu, Z.; Wang, L.; Li, Y. Thermo responsive bilayer hydrogel with switchable bending directions as soft actuator. *Polymer* **2022**, *253*, 124998.

https://doi.org/10.1021/acsapm.4c00536
ACS Appl. Polym. Mater. 2024, 6, 5890−5899